Synsint Research Group

Available online at www.synsint.com

Synthesis and Sintering

ISSN 2564-0186 (Print), **ISSN** 2564-0194 (Online)

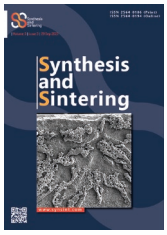

Research article

Ablation behavior of ZrB_2–SiC–Si composites with WC and $MoSi_2$ additives coated through SPS on graphite

Mehran Jaberi Zamharir [a], **Mohammad Zakeri** [a,*], **Zahra Jahangiri** [b], **Ahad Mohammadzadeh** [c]

[a] *Ceramics Department, Materials and Energy Research Center, Karaj, Iran*
[b] *Department of Nano Technology and Advanced Materials, Materials and Energy Research Center, Karaj, Iran*
[c] *Imdea Materials Institute, Calle Eric Kandel, 2, 28906, Getafe, Madrid, Spain*

ABSTRACT

The intention of this paper is to investigate the resistance to ablation of shielding composite coatings built with ultra-high temperature ceramic materials on graphite substrate. To apply the coating on the graphite, the spark plasma sintering route was employed. The applied monolayer coatings had the base compositions of ZrB_2–SiC–Si with the additives of WC and $MoSi_2$, both in the same contents of 1.25 and 3.75 vol%. The outcomes achieved from the ablation tests by oxyacetylene flame showed that applying the protective composite coatings notably enhances the resistance to ablation of the substrate made of graphite. The coating containing more of WC and $MoSi_2$ additives had better performance in terms of ablation resistance in 30–210 seconds. The formation of an oxide layer of $(Zr,Si)O_2$ at the beginning of the ablation process and creating a layer with a porous microstructure on the composite coating surface functioned as a barrier against the destruction and erosion of the inner parts during longer ablation times.

KEYWORDS

UHTCs
Ablation resistance
Graphite
Additive content
Composites coating
Spark plasma sintering

OPEN ACCESS

1. Introduction

Carbonaceous materials, including carbon-carbon and graphite composites, have been very important in recent decades due to their specific applications, such as their use in airplanes, supersonic spacecraft, biology, furnace elements, and space shuttles [1–4]. Generally, in cases where wear resistance is caused by severe flow of very hot and corrosive gases, good specific strength, and the unworkability of cooling systems are needed, such materials can be considered as good candidates [5–8]. Carbon materials have high temperature tolerance, good resistance to fatigue and wear, excellent machinability and shock resistance, low specific weight, high elastic modulus, and ductile fracture [9–12].

The general limitation of carbon, and specifically graphite, parts is their harsh oxidation at temperatures over 400 °C in oxidizing atmospheres. Thus, the successful use of graphite in high temperatures and oxidizing atmospheres necessitates the prohibition of oxidation reactions. Therefore, it is recommended to use coatings that can withhold the oxidation of carbonaceous substrates for a long time [13–15]. To hinder the oxidation of carbon materials, ceramic coatings are used extensively. Among ceramics, the class of ultra-high temperature ceramics (UHTCs) are sublime as coatings due to their fantastic properties such as high tempering temperature, high oxidation resistance, and favorable mechanical behavior. In such coatings, as an outcome of high temperature oxidation, a film of SiO_2 is synthesized that hinders the oxidation of the inner regions [16–21].

Various routes are used to make UHTC coatings. For instance, the modern spark plasma sintering (SPS) is of interest because of creating an appropriate connection with the graphite substrate, the feasibility of controlling the coating thickness, the long life of the coating, and

* Corresponding author. *E-mail address:* m.zakeri@merc.ac.ir (M. Zakeri)
Received 20 August 2023; Received in revised form 25 September 2023; Accepted 25 September 2023.

https://doi.org/10.53063/synsint.2023.33173

having favorable thermo-mechanical properties. These thick and dense coatings are applied to improve toughness, boost wear and corrosion resistance, and inhibit graphite oxidation [22–24]. Applying UHTC coatings on carbon-carbon composites for oxidation resistance enhancement is an acceptable approach to designing thermal protection systems. The coating should be engineered to have the following properties:

-Stable and integrated (continuous) to resist ablation and limit evaporation.

-Preventing oxygen diffusion from the coating to the substrate.

-Mechanical adaptation to resist spallation because of a mismatch in thermal expansion coefficients.

-Reproducible and reliable [25–28].

To boost the ablation resistance of carbon-carbon composites, ZrB_2–SiC coatings prepared by pack cementation have been used. The composition of the powder mixture for the coating process included 45-55 wt% ZrB_2, 7–8 wt% Al_2O_3, 35–45 wt% Si, and 2–3 wt% graphite. The sintering operation was carried out at 1900–2100 °C with a 5 °C/min heating rate for 2 h dwell time in an electric furnace under the argon atmosphere. The results disclosed that the coated samples had outstanding ablation properties compared to the uncoated carbon/carbon composites [29].

To protect the substrate, ZrB_2–SiC composite coatings along with WC and HfB_2 additions were applied on graphite by SPS, and the effects of added materials on coating ablation behavior, microstructure, and phase changes after ablation at high temperature were investigated. The SPS process was performed at 1950 °C under 25 MPa for 30 min. According to the SEM images, the coating thickness and the silicon penetration depth were 500 and 250 μm, respectively. The outcomes of the ablation test with oxyacetylene flame disclosed that the ablation resistance of graphite substrate with protection was meaningfully better than the non-protected substrate. Gaseous byproduct evaporation over the flame test resulted in the decline of flame energy and led to the composite coating remaining unaffected for a long time. The good thermal conductivity of the coating because of the addition of HfB_2 led to the loss of the flame energy, lessened the overall surface temperature, and increased the ablation resistance [24].

The role of the HfB_2/WC ratio on the ablation behavior of graphite substrate, SPS-coated with ZrB_2–SiC–HfB_2–WC composite, was investigated. The specimen with 5 vol% WC and 2.5 vol% HfB_2 significantly had a better ablation resistance. The synthesis of the amorphous silicate phase on the coating surface enhanced the oxidation resistance. The most important mechanism, that led to the improvement of ablation response, was the evaporation of SiO and WO_3 caused by the oxidation of SiC and WC [30].

The ZrB_2–SiC coating was created on the graphite substrate by SPS, which was previously coated with SiC by pack cementation route. Then, the resistance to ablation of the coating against the oxyacetylene flame was investigated at different times. The weight of the samples increased after ablation due to the formation of oxide byproducts. The ZrO_2 film formed from the oxidation of ZrB_2 itself functioned as the thermal barrier. After ablation for 6 min, the inner SiC layer evaporated after being oxidized, and then, created a gap between the graphite and zirconia layer. On the other hand, phase changes of ZrO_2 led to cracks in the central part during the cooling [31].

The goal of current research is to scrutinize the effect of $MoSi_2$ and WC additions to the ZrB_2–SiC–Si coating, both in the same amounts of 1.25 and 3.75 vol%, on the ablation response of the substrate made of graphite. A large part of this paper is devoted to the microstructural investigations after the flame test.

Table 1. Compositions of protective UHTC coatings (reused with permission from Ref. [32]).

	Coating components (vol%)				
Specimen code	**ZrB_2**	**SiC**	**Si**	**WC**	**$MoSi_2$**
ZSS-1.25WM	68.16	14.67	14.67	1.25	1.25
ZSS-3.75WM	64.66	13.92	13.92	3.75	3.75

2. Experimental procedure

In this work, the composite coatings were created by SPS technology on the graphite substrates, the relevant details of which are fully explained in the recent publications of our group [23, 32, 33], and were subjected to ablation test. The results of this test and the microstructure of composite coatings exposed to oxyacetylene flame were studied. In Table 1, the sample code and chemical composition of each composite coating are given.

The ablation behavior of composite coating was investigated by oxyacetylene flame test including oxygen (99.2% purity) and acetylene (98% purity). The nozzle distance to the sample surface, nozzle diameter, measured flame temperature, measured sample surface temperature, and test durations were 10 mm, 2 mm, 2000 °C, 1800 °C, and 30 s, 60 s, 90 s, 150 s, and 210 s, respectively. The mass reduction (ΔW) was calculated based on the following formula:

$$\Delta W\% = \frac{m_0 - m_1}{m_0} \times 100 \quad (1)$$

where m_0 and m_1 are the specimen weights before and after ablation, respectively.

An Eclipse MA100 compact inverted microscope (made by Nikon, Japan) was used in different magnifications for microstructural investigations, observing the surface and cross-section of the specimens subjected to ablation and the curvature of the flame-affected areas. Also, in order to examine the coating microstructure, a Mira3 scanning electron microscope (manufactured by Tescan Co. in The Czech Republic). Meanwhile, for elemental analysis of the specimens, an EDS detector was also used.

3. Results and discussion

The amounts of mass reduction of the specimens subjected to the ablation test at different times are given in Table 2. The mass reduction of samples with protective composite coating is much lower than the specimen with no protection. Thus, it can be concluded that the ablation resistance of the protected graphite substrate is greater than graphite without coating. Also, from the comparison of the values obtained from the ablation test, the ZSS-3.75WM specimen has the lowest mass reduction and therefore the best performance in ablation resistance.

The changes due to the oxyacetylene exposure on the surface of ZSS-1.25WM and ZSS-3.75WM composite coatings, after 90 and 210 s ablation, are depicted in Fig. 1. In the ZS-1.25WM sample, because of the flame hitting the surface of the coatings, the remnants of the flame were concentrated in one part. In addition, melting in the center of the

Table 2. Mass reduction after ablation test in substrate made of graphite and UHTC coated specimens**.**

Specimen code	Ablation test time				
	30 s	60 s	90 s	150 s	210 s
ZSS-1.25WM	0.6±0.0%	1.1±0.1%	1.7±0.1%	2.9±0.1%	3.8±0.1%
ZSS-3.75WM	0.3±0.0%	0.6±0.0%	1.1±0.0%	2.4±0.1%	3.1±0.1%
Graphite substrate	7.1±0.3%	12.2±0.5%	15.3±0.7%	21.1±1.0%	30.2±1.2%

coating and detachment from the composite coating were observed. On the contrary, in the ZS-3.75WM sample, the remnants of the flame were spread on the surface of the coating. As the exposure duration enhances, the level of flame destruction increases, which leads to melting, cracking, detachment, and fracture on the coating surface to increase.

The macroscopic image of the ZSS-1.25WM coating surface after performing the flame exposure for 210 s, as well as the optical microscope images of different regions of the surface of this sample, are presented in Fig. 2. As seen in Fig. 2a, the surface of the coating of this sample can be divided into three regions based on the degree of destruction and erosion: (1) the edge, (2) the middle and (3) the central parts. In this sample, in addition to cracks and fractures, melting and fundamental changes in the surface microstructure have also occurred. In the optical microscope image of Fig. 2b, which is related to the edge of this sample, no drastic changes have been made and only parts of it that are near the middle region have undergone surface oxidation, which is characterized by the formation of a white oxide layer. Fig. 2c corresponds to the middle region of the composite coating surface that has undergone changes in the microstructure and has more melted parts as well as ups and downs. These observations are because of the evaporation of gaseous byproduct released through chemical reactions and the surface oxidation of weak phases because of the considerable heat of the oxyacetylene flame. The images in Figs. 2d–f belong to the center of this specimen, which has the greatest level of erosion due to the flame, which also caused a lot of melting and detachment in addition to the fundamental changes in the microstructure .

Fig. 3 illustrates the optical microscope cross-sectional images of the ZSS-1.25WM specimen after the flame test for 210 s. Two regions with different structures and color contrast can be seen in this figure, the upper part is related to the composite coating, and the lower part is related to the graphite. In the coating belonging to the center of the cross-section of the ZSS-1.25WM specimen (Figs. 3c and d), there is a strong gradient in thickness, which is caused by the erosion and destruction of the coating due to the flame. In other words, detachment occurred remarkably in this region, but erosion and reduction in the

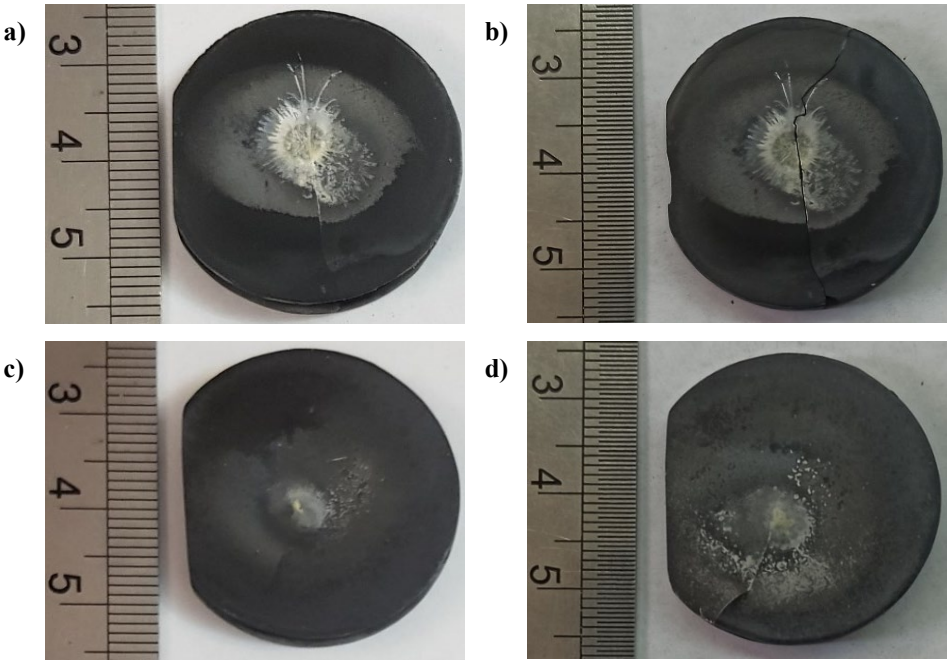

Fig. 1. Macroscopic images of the composite coating surfaces of the samples: a, b) ZSS-1.25WM and c, d) ZSS-3.75WM, subjected to oxyacetylene flame for 90 s and 120 s, respectively**.**

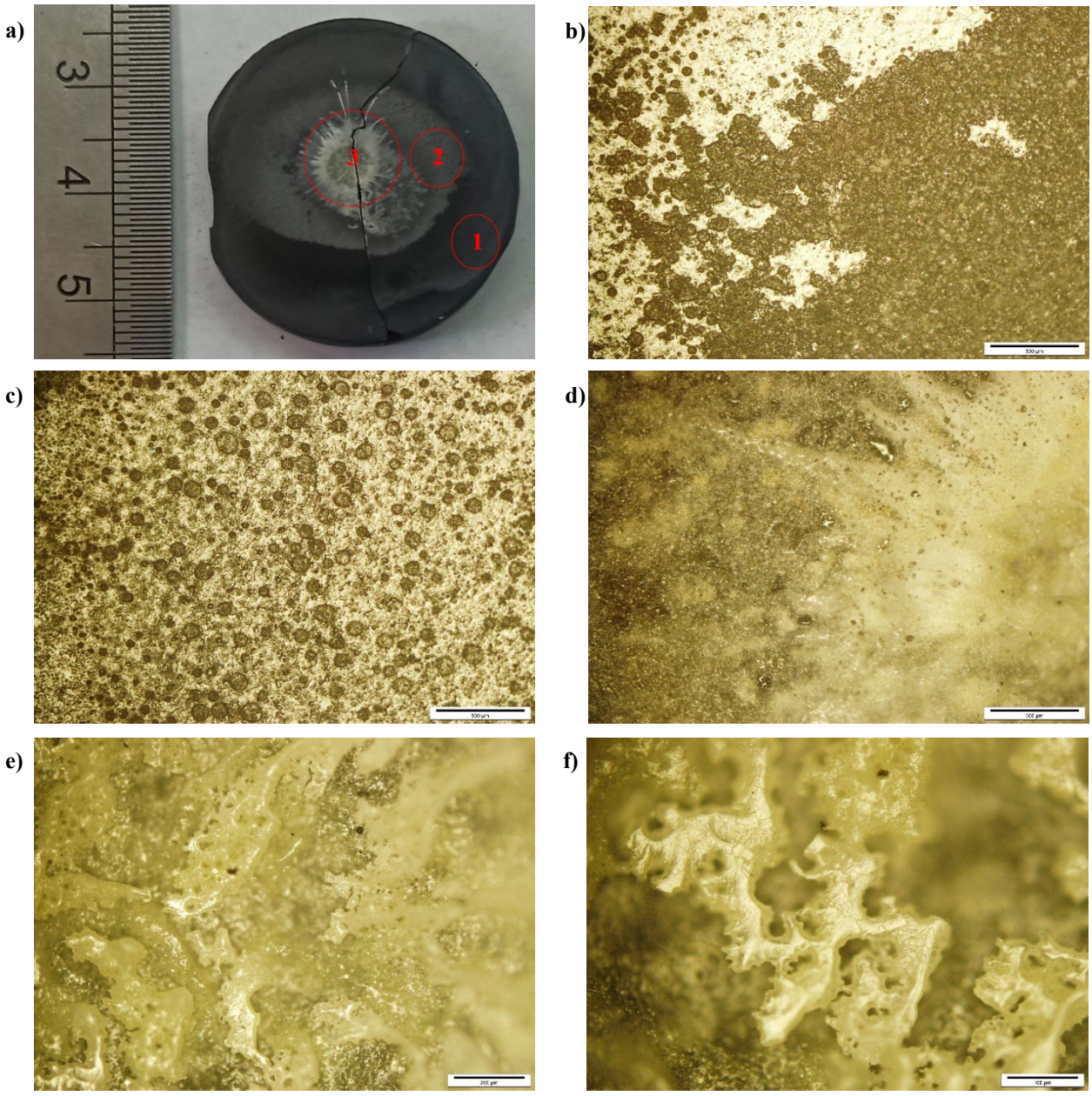

Fig. 2. a) Macroscopic image of the surface of ZSS-1.25WM specimen after ablation test, and optical microscope images of b) region 1: the edge part, c) region 2: the middle part and d–f) region 3 of the central part marked in Fig. 2a.

coating thickness at the edge were insignificant and uniform. It should be noted that in the middle part, the erosion and thickness reduction has intensified by approaching the central region (Fig. 3b).

Fig. 4a shows the macroscopic image (taken by SEM) of the ZSS-1.25WM coating surface exposed for 210 s to flame. Fig. 4b displays an image with higher magnification of the central part of this sample, which has suffered severe destruction and microstructural changes. In this part, in addition to intense melting, a porous structure containing a large number of holes has been created. Fig. 4c depicts an image of the middle part of this sample, which is less involved in ablation than the central region. However, in this part, in addition to melting, detachment from the surface is also seen.

To investigate more precisely the microstructure of the destroyed central part of the ZSS-1.25WM specimen, SEM images with higher magnification were taken. As shown in Fig. 5, two microstructurally different parts in the central part were investigated. In the SEM image shown in Fig. 4b, region(s) B can be seen next to region(s) A, where region B is raised, and region A is sunk. As can be seen in Figs. 5a and

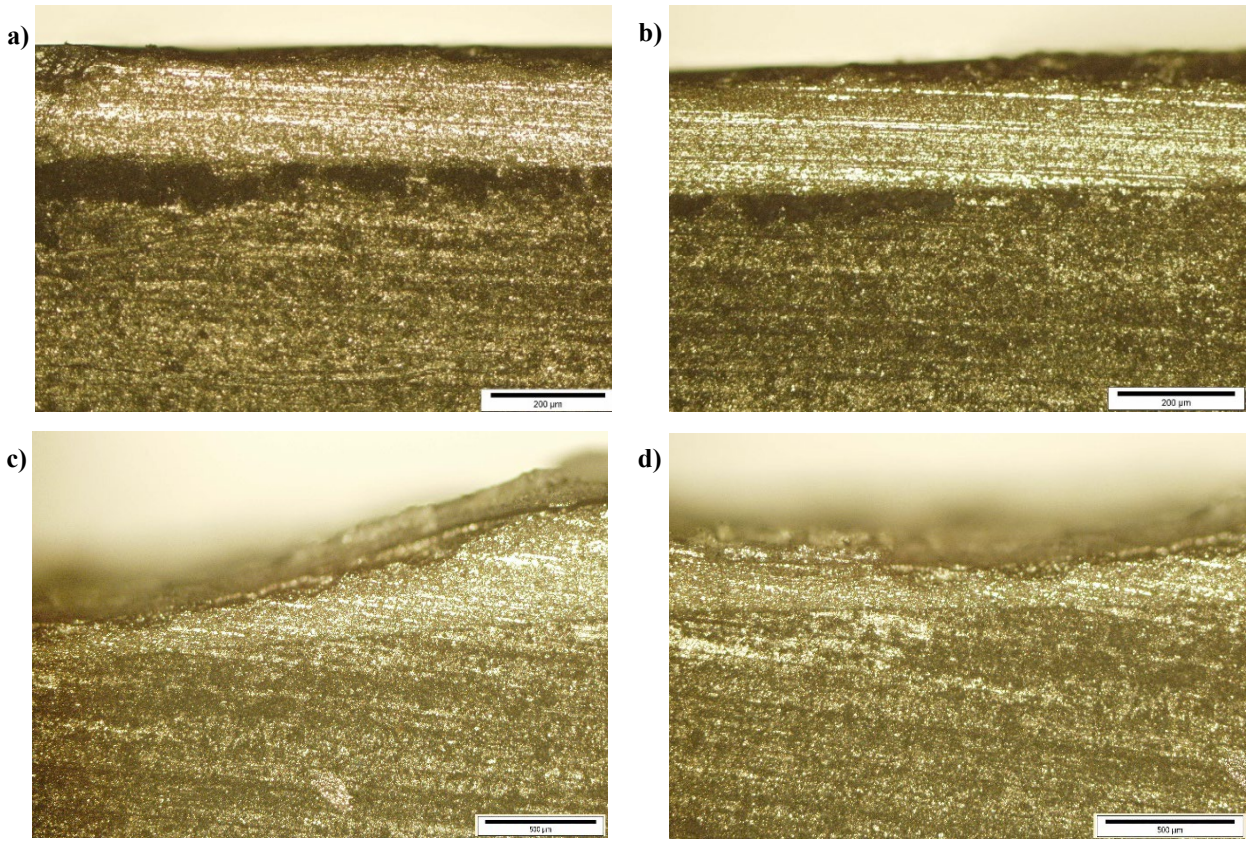

Fig. 3. Optical microscope images from the ground surface to the center of the ZSS-1.25WM coating after the ablation test, a) the edge part, b) the middle part, and c, d) the central part.

b, region A and similar areas have a microstructure with surface-melted grains and a large number of holes. These holes are formed as a result of the release of gases coming from the raw materials oxidation that make up the coating of the lower parts. Region B and similar zones have a large number of holes, cracks, and recrystallization of grains in an irregularly and randomly on the frozen parts after melting.

Fig. 6 shows the SEM data of the ZSS-1.25WM surface at the interface of the central/middle parts. To review the microstructural changes caused by the flame test, the images with higher magnification taken from region C indicated with a red square in Fig. 6a, were used. As seen in Figs. 6b and c, this region has two distinct structures: the darker part that is melted and formed as an amorphous layer with holes, and the lighter part that has an irregularly recrystallized microstructure that includes many pores. For a more detailed examination of the recrystallized part, an image with higher magnification (Fig. 6d) was used, which shows that a series of new grains of different phases are formed on the frozen molten phase. Recrystallization of zirconia was also detected by Zhang et al. [34] during the ablation process for 2 min. By increasing the exposure time, the surface of the samples is exposed to elevated temperatures for a longer time; hence, the grain growth is higher.

Fig. 7 shows the elemental distribution maps obtained from the EDS analysis taken from the interface between the middle and central areas of the ZSS-1.25WM flame-affected sample. In this analysis, red, green, yellow, purple, turquoise, and blue colors represent the elements of zirconium, silicon, oxygen, molybdenum, tungsten, and carbon, respectively. The Mo, W, and C elements are distributed in almost all regions. The concentration of the Si element in the upper part of the image, which shows the central part of the sample, is much lower than in the lower part of the image, which represents the middle part of the sample. The central part of the sample was directly affected by the flame and experienced a higher temperature. Therefore, phases containing Si elements such as SiO_2, which are the result of oxidation of SiC and $MoSi_2$, are melted, evaporated, and finally removed from this part.

It should be noted that in the early stages of ablation, the synthesis of oxide phases like SiO_2 and ZrO_2 resulting from the oxidation of raw materials on the coating surface plays an essential role in hindering the oxidation of inner parts. Here, due to the elevated temperature of the flame and the lower melting temperature of SiO_2 compared to ZrO_2, the SiO_2 has melted and then evaporated. For this reason, the Zr concentration is high in this area, which indicates the presence of the ZrO_2 protective layer formed due to the oxidation of ZrB_2 because of the flame's elevated temperature.

The cross-sectional SEM data of the ZSS-1.25WM specimen after exposure for 210 s to oxyacetylene flame is shown in Fig. 8. The sample center (Fig. 8a) is severely damaged and has a sharp thickness gradient. It is clear that the minimum coating thickness in the central

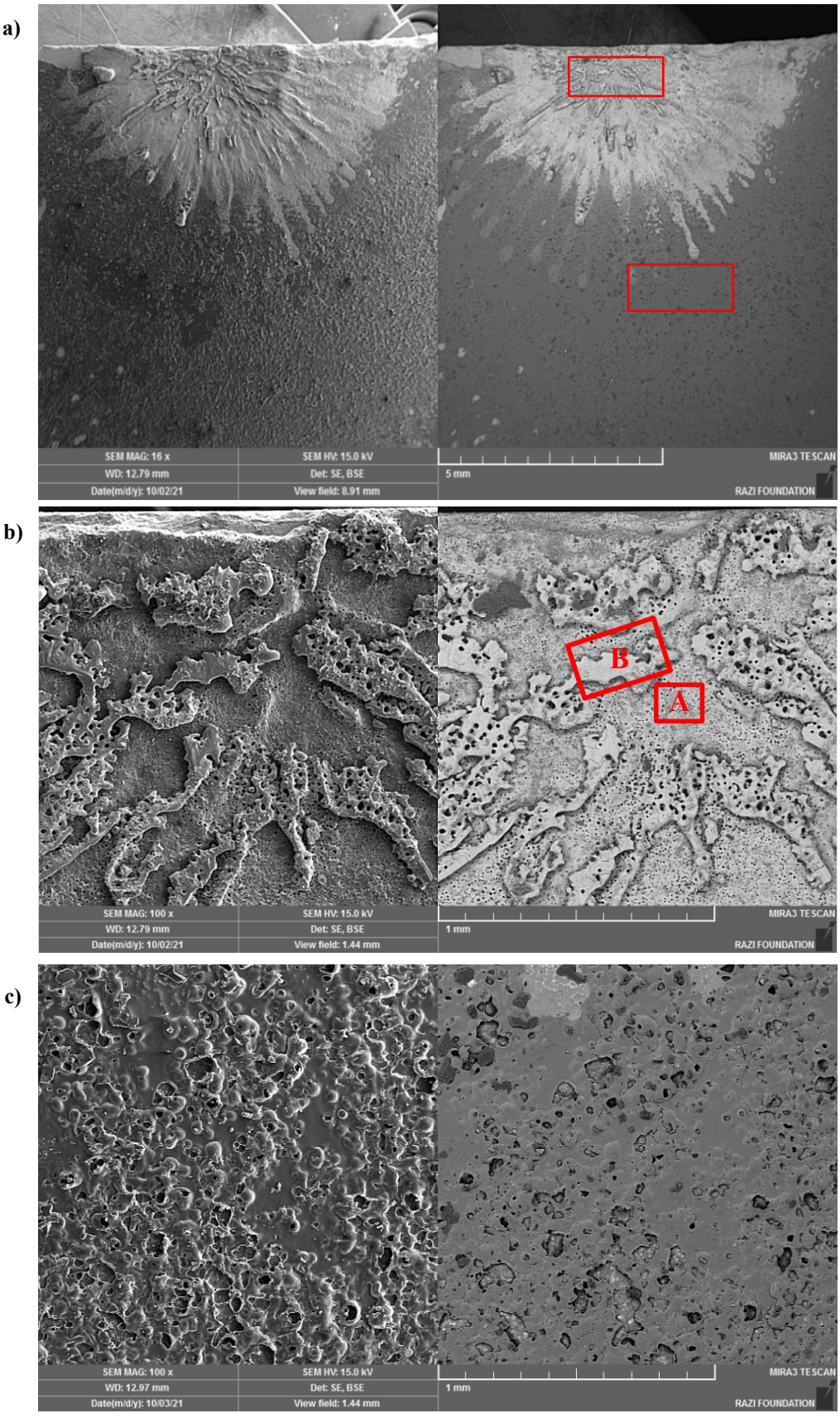

Fig. 4. SEM images of the ZSS-1.25WM sample a) surface exposed to flame, b) central part and c) middle part.

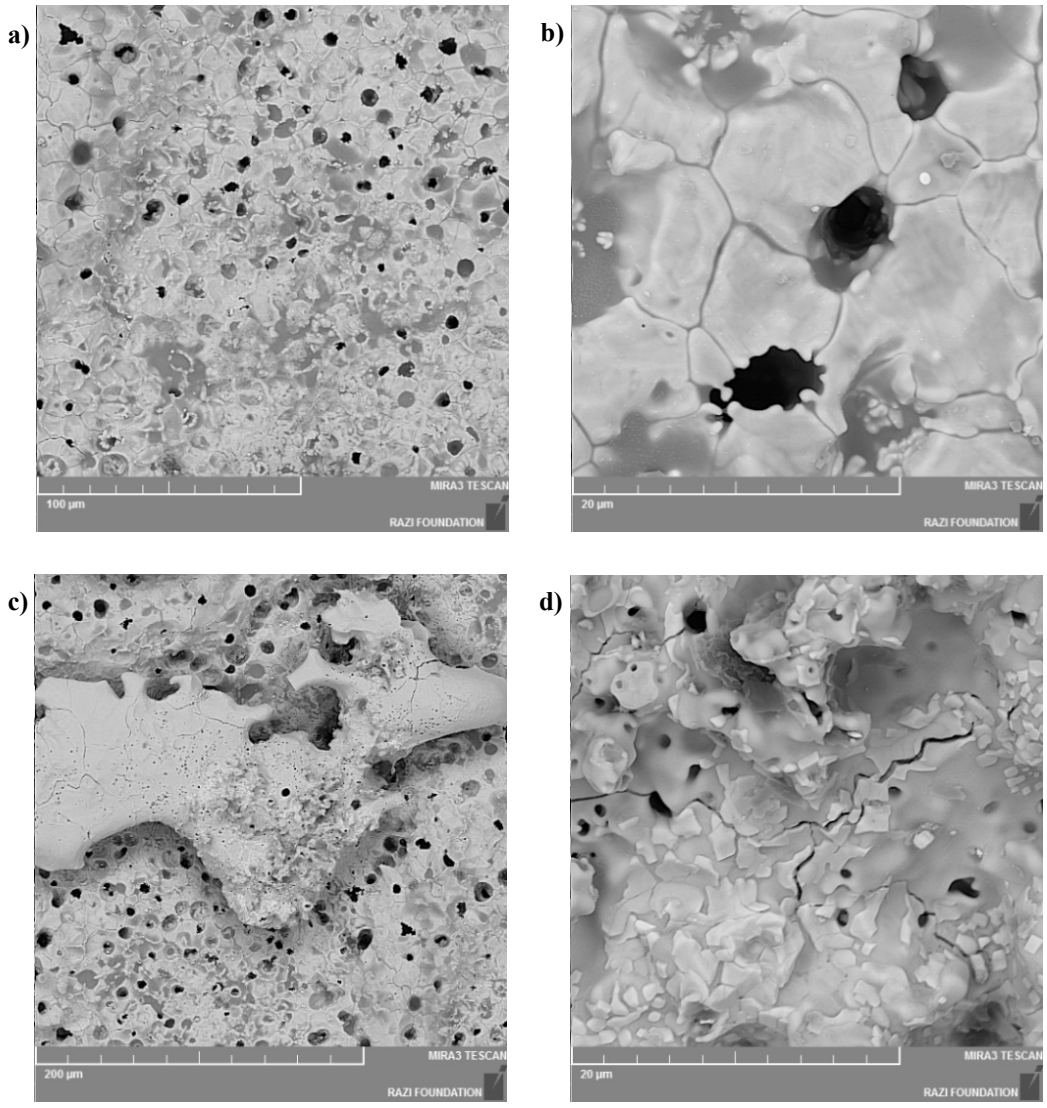

Fig. 5. SEM images with higher magnification taken from a, b) zone A and c, d) zone B in Fig. 4b.

zone is about 230 µm. According to Fig. 8b, the thickness in the middle parts is approximately 430 µm. It is worth mentioning that the initial coating thickness before the ablation study was about 440 µm in the entire sample [32], which suffered a thickness gradient due to ablation with oxyacetylene flame. In fact, by moving from the edge to the center, the thickness of the coating is reduced, as the central zone has minimal thickness.

To examine the cross-section of the ZSS-1.25 WM center more accurately after the flame test for 210 s, elemental map analysis was used. Fig. 9 shows the SEM/EDS data of the central zone with a sharp thickness gradient. From the high concentration of oxygen on the inclined part compared to other regions, it is clear that an oxide layer is formed there, which behaves as a barrier against oxidation of the internal areas. Also, from the way of elemental distributions of Zr, W, and Mo and relatively high concentrations of oxygen in the triangular part of the upper area, it can be concluded that oxide phases are formed including these elements. On the other hand, due to the high concentration of Zr element, the formation of the ZrO_2 protective layer is somehow confirmed. From the distribution map of the Si, it can be seen a high concentration of this element at the interface of the graphite substrate/composite coating and also up to a specific thickness of the substrate. Considering the high temperature of the flame and the low melting point of Si, the reason for the high concentration of Si element in the mentioned parts is that Si has melted and due to the capillary force has penetrated through the existing open pores to the inner parts and even inside the graphite substrate.

With the increase of the flame test time and the propagation of ablation, the white layer created in the central and middle areas of the coating surface has developed (Figs. 2a and 4a). The applied layer can include the oxidation byproducts of the

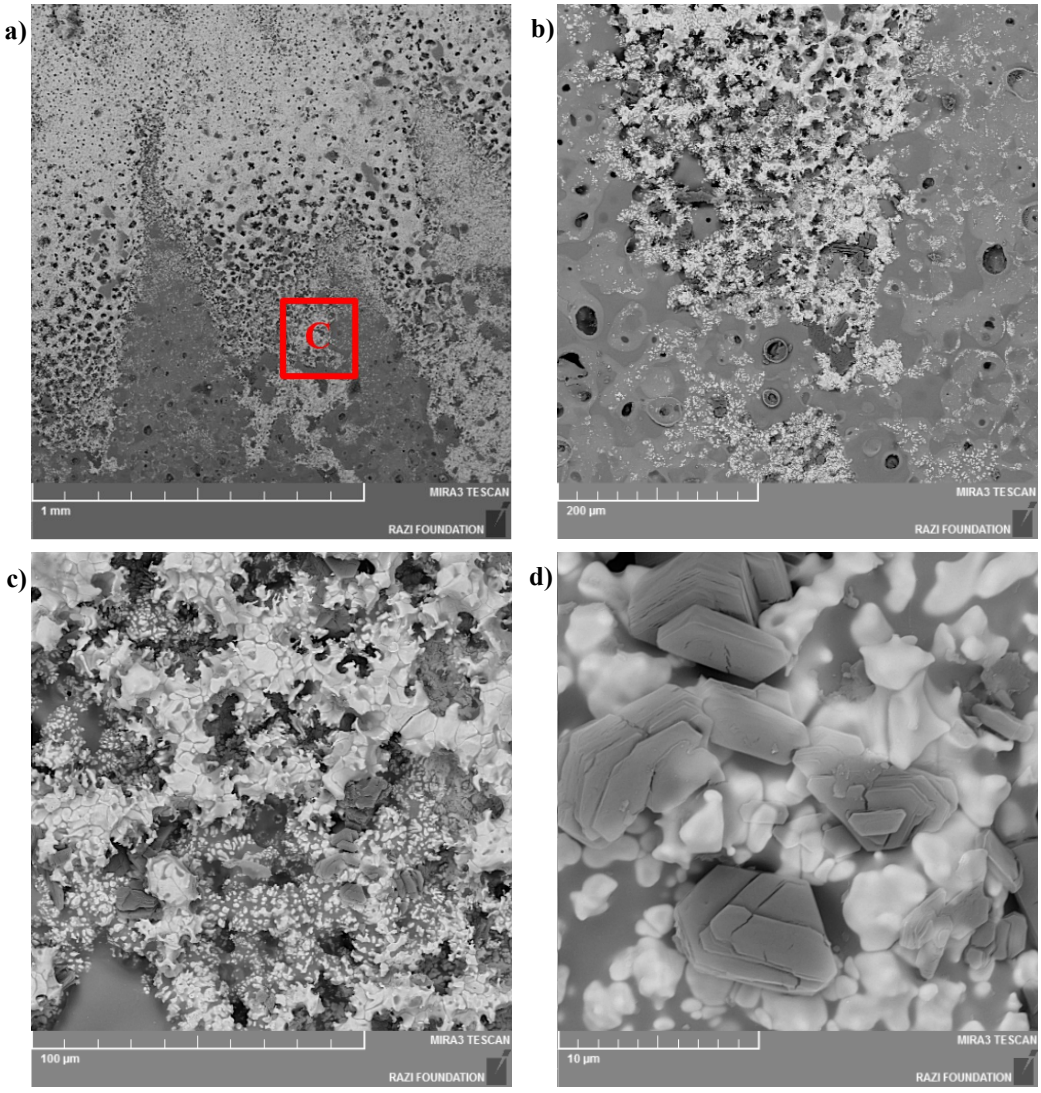

Fig. 6. SEM images of the interface of the central/middle areas of ZSS-1.25WM sample in different magnifications.

starting materials used in making the coating. Meanwhile, according to the results obtained from elemental map analysis (Figs. 7 and 9), this oxide layer is made of ZrO_2 and has developed over time and its thickness has also increased. At the same time, large cracks on the surface (Figs. 2a and 5d) and the cross-section (Fig. 9a) have been created and the detachment of the oxide layer is visible. The formation of cracks and the detachment of the layer from the surface is the outcome of the stresses caused by the cooling of the samples from high temperatures. Also, the temperature differences between the central and other regions of the specimen during the cooling step may result in stresses and generate cracks. Additionally, during the cooling process, the phase transformation of tetragonal monoclinic ZrO_2 occurs [35], which causes expansion [36]. The cracks detected in the samples are mainly caused by such volume increase. Finally, the cracks gradually expand and cause the detachment of the oxide layer from the below composite coating.

Fig. 10 illustrates the SEM images taken from the composite coating surface of the ZSS-3.75WM sample after 210 s ablation. According to Fig. 10a, the central part has the highest amount of erosion and destruction. In addition to microstructural changes, melting and recrystallization during cooling can also be seen. For a more detailed examination of the microstructural evolution that happened in the central part of the sample, an image with higher magnification was taken (Fig. 10b). This part consists of an amorphous layer with many cracks and holes. The holes were created because of the release of gaseous byproducts via reactions of oxidation. The cracks were probably caused by the stresses over the rapid cooling after the test.

The SEM data of the ZSS-3.75WM cross section after exposure for 210 s to oxyacetylene flame are shown in Fig. 11. Because

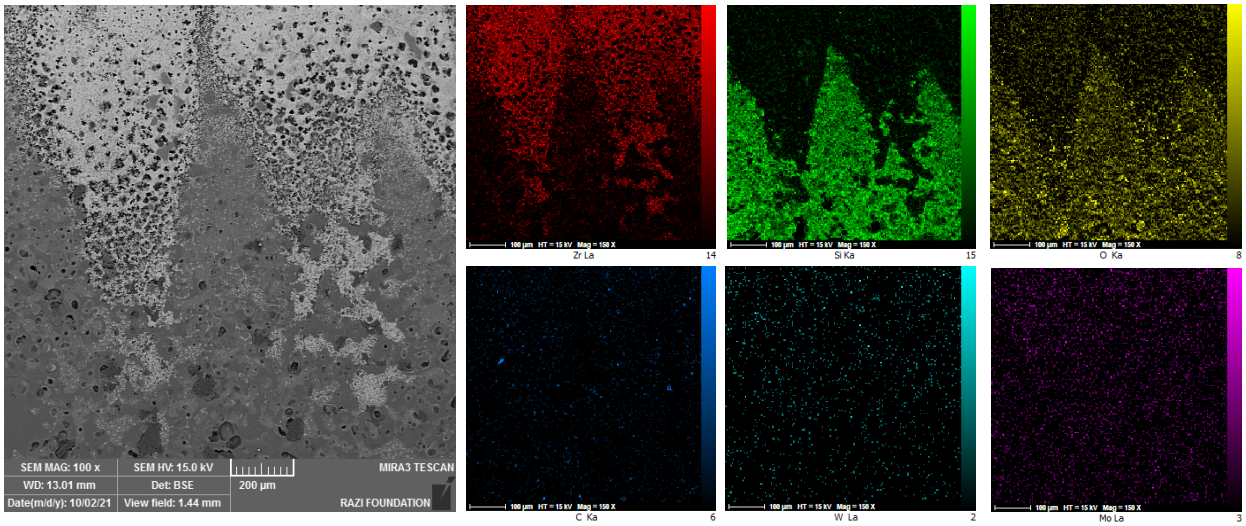

Fig. 7. SEM/EDS analyses taken from the interface between the middle and central zones of ZSS-1.25WM sample.

the coating thickness before the flame test was approximately equal to 690 µm [32], according to Fig. 11, it can be seen that the thickness reduction in the middle and central areas is approximately the same without extreme thickness gradient.

EDS map data was used to study the intensity of ablation in the central part of the ZSS-3.75WM specimen. Fig. 12 depicts the SEM image of the center and the interface of the middle/central areas of the ZSS-3.75WM coating surface as well as the results of the EDS analysis obtained from these areas. The distribution of Mo, W, and C are almost the same in all areas. The concentration of Si element is low in the central part, which has melted and recrystallized, and on the other hand, the intensity of this element is high in the lower parts and near the interface of the central/middle regions. Due to the concentration of oxygen in the area close to the interface, the possibility of SiO_2 phase formation is high. On the other hand, the high concentration of Zr element is significant in the parts with a lower concentration of Si. The concentration of zirconium is high in the central part, which has the maximum ablation and has undergone melting and recrystallization.

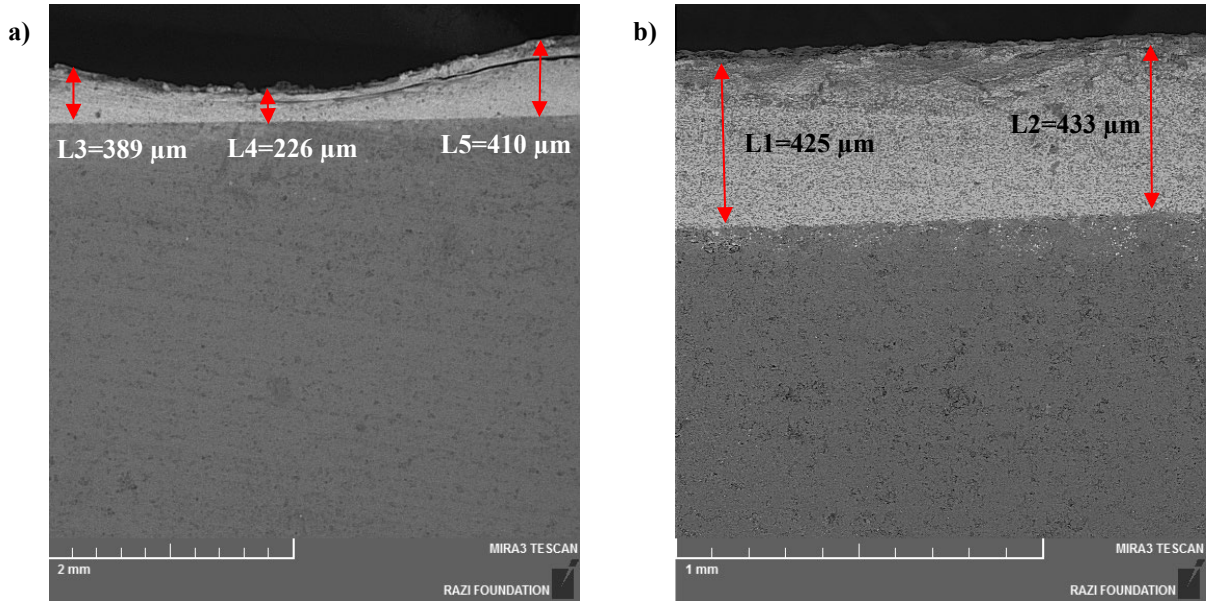

Fig. 8. SEM images of the ZSS-1.25WM cross-section after exposure for 210 s, a) central part and b) middle part.

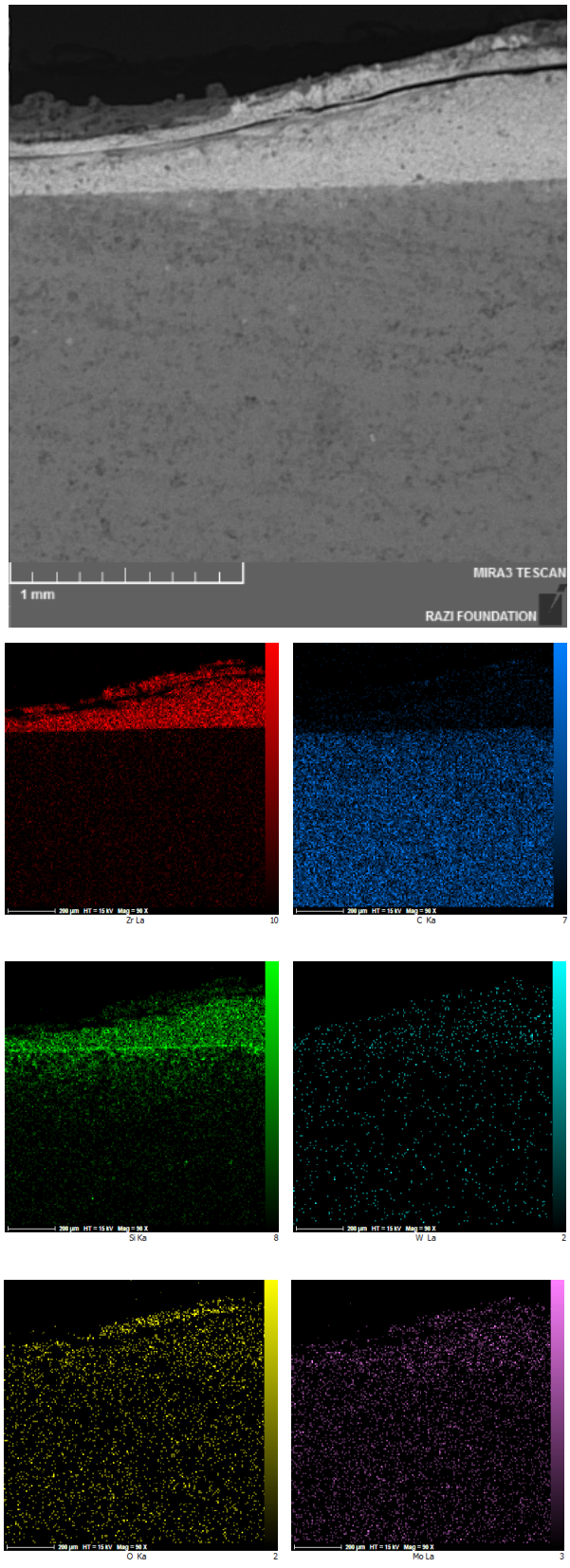

Fig. 9. Cross-sectional SEM/EDS data of the ZSS-1.25WM center after exposure for 210 s.

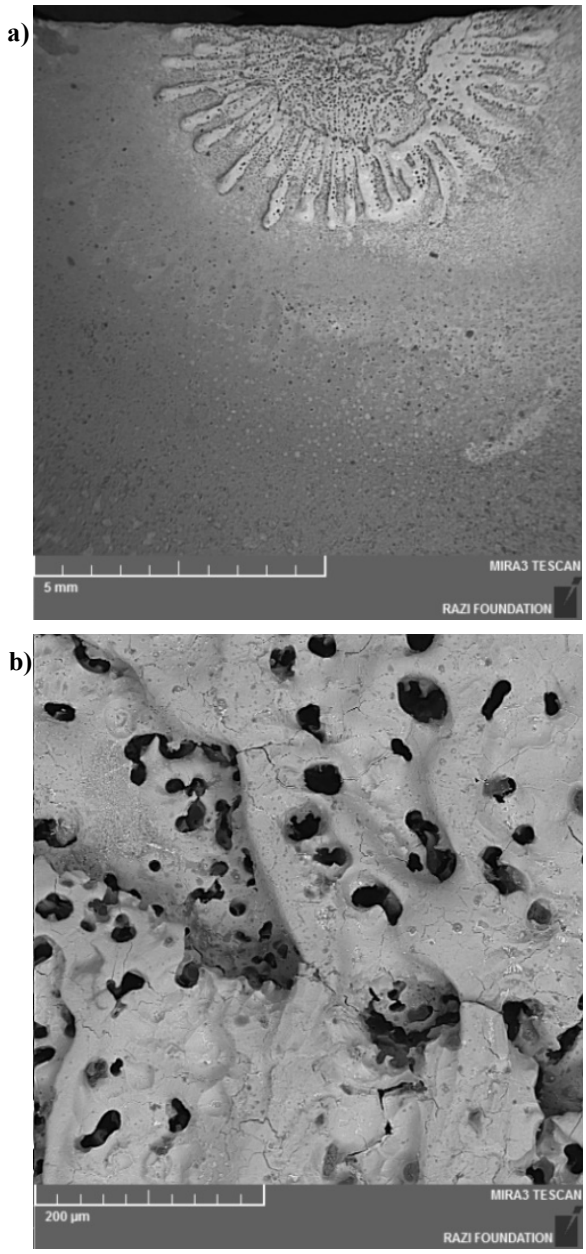

Fig. 10. SEM images of a) the surface of ZSS-3.75WM specimen and b) the central part in high magnification exposed to oxyacetylene flame for 210 s.

The concentration of oxygen in this region also indicates the formation of the ZrO_2 phase. Perhaps, from this observation, it can be concluded that because of the low melting and boiling temperature of SiO_2, this oxide has been removed from the coating center because of the flame's high temperature. However, due to the high refractoriness of the ZrO_2 compared to SiO_2, zirconia is still seen in the central zone.

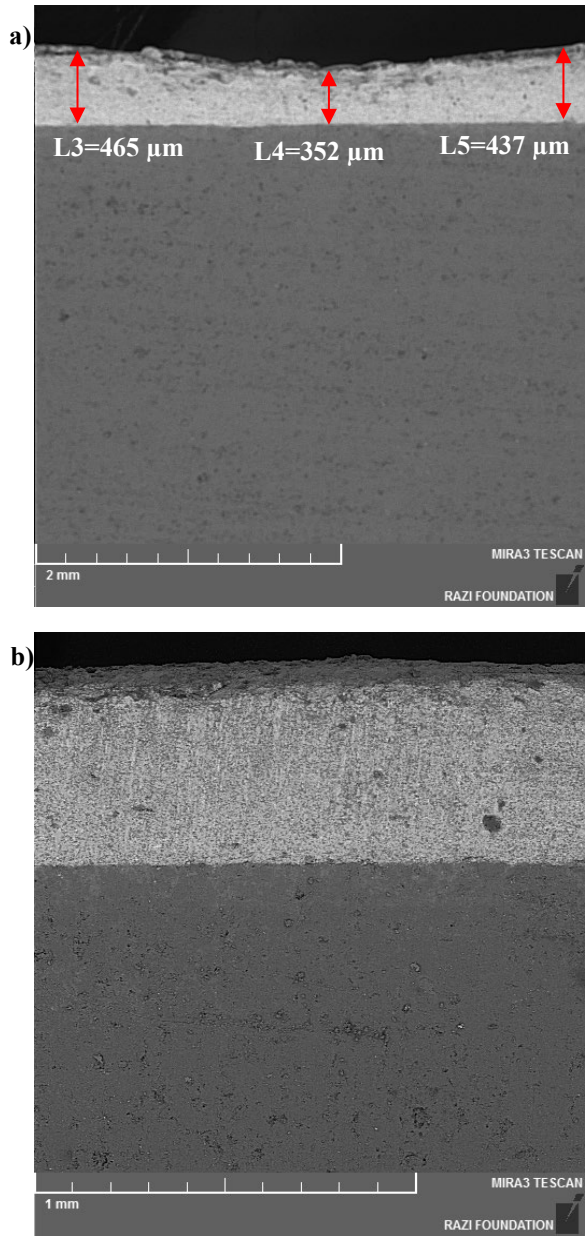

Fig. 11. SEM data of the cross-sectional surface of ZSS-3.75WM sample after flame test for 210 s, a) center and b) middle zone.

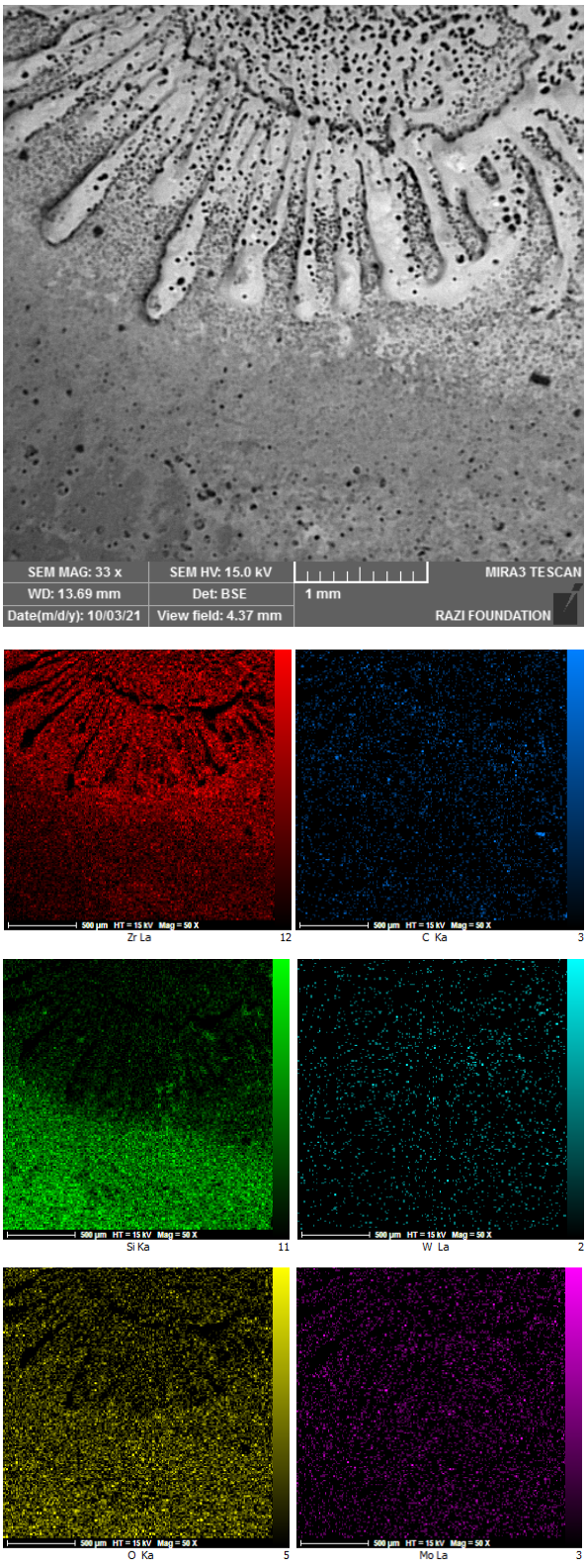

Fig. 12. SEM/EDS data taken from the center and the interface between the middle and central parts of ZSS-3.75WM specimen after 210 s ablation.

4. Conclusions

In this work, UHTC-made coatings based on ZrB_2–SiC–Si composites and WC and $MoSi_2$ additives were applied on graphite substrates by the SPS method to promote ablation resistance. Based on the outcomes, the specimens with protective coating have a lesser mass reduction and therefore a high resistance to ablation compared to the substrate with no protection. The coating containing WC and $MoSi_2$ additives with 3.75 vol% of each showed the best performance against ablation. The presence of these additives in the coating caused new phases of synthesis during the SPS process. During the ablation test, these phases

caused flame energy loss by catching the heat of the flame, oxidizing, and eventually vaporizing, and also by spreading the heat of the flame due to their high thermal conductivity. In fact, they somehow sacrificed themselves to protect the main body of the composite coating.

CRediT authorship contribution statement

Mehran Jaberi Zamharir: Investigation, Project administration, Conceptualization, Data curation, Formal Analysis, Writing – original draft.
Mohammad Zakeri: Funding acquisition, Supervision, Validation, Writing – review & editing.
Zahra Jahangiri: Investigation, Writing – original draft.
Ahad Mohammadzadeh: Formal Analysis, Writing – review & editing.

Data availability

The data underlying this article will be shared on reasonable request to the corresponding author.

Declaration of competing interest

The authors declare no competing interests.

Funding and acknowledgment

This article is derived from the PhD thesis of the first author, bearing tracking code 1464813 at the Iranian Research Institute for Information Science and Technology (IranDoc). The authors wish to extend their deepest gratitude to the Materials and Energy Research Center and all those who provided assistance in the completion of this thesis.

References

[1] Z. Dong, B. Sun, H. Zhu, G. Yuan, B. Li, et al., A review of aligned carbon nanotube arrays and carbon/carbon composites: fabrication, thermal conduction properties and applications in thermal management, New Carbon Mater. 36 (2021) 873–892. https://doi.org/10.1016/S1872-5805(21)60090-2.
[2] F. Muhammed, T. Lavaggi, S. Advani, M. Mirotznik, J.W. Gillespie, Influence of material and process parameters on microstructure evolution during the fabrication of carbon–carbon composites: a review, J. Mater. Sci. 56 (2021) 17877–17914. https://doi.org/10.1007/s10853-021-06401-3.
[3] M. Singh, R. Vander Wal, Carbon - carbon composites: Effect of graphene size upon the nano-micro - structure and material properties, Carbon Trends. 4 (2021) 100061. https://doi.org/10.1016/j.cartre.2021.100061.
[4] J.H. Park, J. Yang, D. Kim, H. Gim, W.Y. Choi, J.W. Lee, Review of recent technologies for transforming carbon dioxide to carbon materials, Chem. Eng. J. 427 (2022) 130980. https://doi.org/10.1016/j.cej.2021.130980.
[5] W. Zhai, L. Bai, R. Zhou, X. Fan, G. Kang, et al., Recent progress on wear-resistant materials: designs, properties, and applications, Adv. Sci. 8 (2021) 2003739. https://doi.org/10.1002/advs.202003739.
[6] R. Soni, R. Verma, R. Kumar Garg, V. Sharma, A critical review of recent advances in the aerospace materials, Mater. Today Proc. (2023). https://doi.org/10.1016/j.matpr.2023.08.108.
[7] K.M. Steel, W.J. Koros, An investigation of the effects of pyrolysis parameters on gas separation properties of carbon materials, Carbon. 43 (2005) 1843–1856. https://doi.org/10.1016/j.carbon.2005.02.028.
[8] P. Baraneedharan, S. Vadivel, C.A. Anil, S.B. Mohamed, S. Rajendran, Advances in preparation, mechanism and applications of various carbon materials in environmental applications: A review, Chemosphere. 300 (2022) 134596. https://doi.org/10.1016/j.chemosphere.2022.134596.
[9] D.E. Wittmer, M.Z. Temuri, Thermochemical studies in selected metal-carbon-oxygen systems, J. Am. Ceram. Soc. 74 (1991) 973–982. https://doi.org/10.1111/j.1151-2916.1991.tb04330.x.
[10] A.A. Balandin, Thermal properties of graphene and nanostructured carbon materials, Nat. Mater. 10 (2011) 569–581. https://doi.org/10.1038/nmat3064.
[11] D.S. Su, G. Centi, A perspective on carbon materials for future energy application, J. Energy Chem. 22 (2013) 151–173. https://doi.org/10.1016/S2095-4956(13)60022-4.
[12] M. Thompson, Q. Xia, Z. Hu, X.S. Zhao, A review on biomass-derived hard carbon materials for sodium-ion batteries, Mater. Adv. 2 (2021) 5881–5905. https://doi.org/10.1039/D1MA00315A.
[13] X. Zhang, B. Du, P. Hu, Y. Cheng, J. Han, Thermal response, oxidation and ablation of ultra–high temperature ceramics, C/SiC, C/C, graphite and graphite–ceramics, J. Mater. Sci. Technol. 102 (2022) 137–158. https://doi.org/10.1016/j.jmst.2021.06.022.
[14] B. Du, Y. Cheng, L. Xun, S. Zhang, J. Tong, et al., Using PyC modified 3D carbon fiber to reinforce UHTC under low temperature sintering without pressure, J. Adv. Ceram. 10 (2021) 871–884. https://doi.org/10.1007/s40145-021-0495-9.
[15] D. Yang, S. Dong, C. Hong, X. Zhang, Preparation, modification, and coating for carbon-bonded carbon fiber composites: A review, Ceram. Int. 48 (2022) 14935–14958. https://doi.org/10.1016/j.ceramint.2022.03.055.
[16] M. Naderi, M. Vajdi, F. Sadegh Moghanlou, H. Nami, Sensitivity analysis of fluid flow parameters on the performance of fully dense ZrB2-made micro heat exchangers, Synth. Sinter. 3 (2023) 88–106. https://doi.org/10.53063/synsint.2023.32143.
[17] X. Zhu, Y. Zhang, Y. Su, Y. Fu, P. Zhang, SiC-Si coating with micro-pores to protect carbon/carbon composites against oxidation, J. Eur. Ceram. Soc. 41 (2021) 114–120. https://doi.org/10.1016/j.jeurceramsoc.2020.08.045.
[18] M. Zhang, X. Ren, H. Chu, J. Lv, W. Li, et al., Oxidation inhibition behaviors of the HfB2-SiC-TaSi2 coating for carbon structural materials at 1700 °C, Corros. Sci. 177 (2020) 108982. https://doi.org/10.1016/j.corsci.2020.108982.
[19] Y. Jiang, S. Yin, M. Li, Z. Zhang, G. Tang, et al., Oxidation and ablation behaviour of multiphase ultra-high-temperature ceramic Ta0·5Zr0·5B2–Si–SiC protective coating for graphite, Ceram. Int. 47 (2021) 11358–11371. https://doi.org/10.1016/j.ceramint.2020.12.262.
[20] J. Binner, M. Porter, B. Baker, J. Zou, V. Venkatachalam, et al., Selection, processing, properties and applications of ultra-high temperature ceramic matrix composites, UHTCMCs – a review, Int. Mater. Rev. 65 (2020) 389–444. https://doi.org/10.1080/09506608.2019.1652006.
[21] Y. Jiang, Q. Ren, H. Ru, Z. Mao, H. Xu, Oxidation protection of graphite materials by single-phase ultra-high temperature boride modified monolayer Si-SiC coating, Ceram. Int. 45 (2019) 539–549. https://doi.org/10.1016/j.ceramint.2018.09.206.
[22] M. Shirani, M. Rahimipour, M. Zakeri, S. Safi, T. Ebadzadeh, ZrB2-SiC-WC coating with SiC diffusion bond coat on graphite by spark plasma sintering process, Ceram. Int. 43 (2017) 14517–14520. https://doi.org/10.1016/j.ceramint.2017.07.123.
[23] M. Jaberi Zamharir, M. Zakeri, M. Razavi, Challenges toward applying UHTC-based composite coating on graphite substrate by spark plasma sintering, Synth. Sinter. 1 (2021) 202–210. https://doi.org/10.53063/synsint.2021.1452.
[24] S.A. Akbarpour Shalmani, M. Sobhani, O. Mirzaee, M. Zakeri, Effect of HfB2 and WC additives on the ablation resistance of ZrB2–SiC composite coating manufactured by SPS, Ceram. Int. 46 (2020) 25106–25112. https://doi.org/10.1016/j.ceramint.2020.06.297.

[25] E.L. Corral, R.E. Loehman, Ultra-high-temperature ceramic coatings for oxidation protection of carbon-carbon composites, J. Am. Ceram. Soc. 91 (2008) 1495–1502. https://doi.org/10.1111/j.1551-2916.2008.02331.x.

[26] X. Jin, X. Fan, C. Lu, T. Wang, Advances in oxidation and ablation resistance of high and ultra-high temperature ceramics modified or coated carbon/carbon composites, J. Eur. Ceram. Soc. 38 (2018) 1–28. https://doi.org/10.1016/j.jeurceramsoc.2017.08.013.

[27] S. Chen, X. Qiu, B. Zhang, J. Xu, F. Zhong, et al., Advances in antioxidation coating materials for carbon/carbon composites, J. Alloys Compd. 886 (2021) 161143. https://doi.org/10.1016/j.jallcom.2021.161143.

[28] L.S. Walker, E.L. Corral, Self-generating high-temperature oxidation-resistant glass-ceramic coatings for C−C composites using UHTCs, J. Am. Ceram. Soc. 97 (2014) 3004–3011. https://doi.org/10.1111/jace.13017.

[29] D. Wang, Y. Zeng, X. Xiong, G. Li, Z. Chen, et al., Preparation and ablation properties of ZrB2–SiC protective laminae for carbon/carbon composites, Ceram. Int. 40 (2014) 14215–14222. https://doi.org/10.1016/j.ceramint.2014.06.010.

[30] S.A.A. Shalmani, M. Sobhani, O. Mirzaee, M. Zakeri, Ablation resistance of graphite coated by spark plasma sintered ZrB2–SiC based composites, Bol. Soc. Esp. Cerám. Vidr. 61 (2022) 604–610. https://doi.org/10.1016/j.bsecv.2021.05.004.

[31] R. Aliasgarian, M. Naderi, S.E. Mirsalehi, Ablation mechanism of ZrB2-SiC coating for SiC-coated graphite under an oxyacetylene flame, Surf. Coat. Technol. 350 (2018) 511–518. https://doi.org/10.1016/j.surfcoat.2018.07.031.

[32] M. Jaberi Zamharir, M. Zakeri, Z. Jahangiri, A. Mohammadzadeh, Microstructural characterization of ZrB2–SiC–Si–MoSi2–WC coatings applied by SPS on graphite substrate, Synth. Sinter. 3 (2023) 124–131. https://doi.org/10.53063/synsint.2023.32152.

[33] M. Jaberi Zamharir, M. Shahedi Asl, M. Zakeri, M. Razavi, Microstructure of spark plasma coated ultrahigh temperature ZrB2–SiC–Si composites on graphite substrate, Silicon. 15 (2023) 6015–6024. https://doi.org/10.1007/s12633-023-02475-7.

[34] Y. Zhang, H. Hu, P. Zhang, Z. Hu, H. Li, L. Zhang, SiC/ZrB2–SiC–ZrC multilayer coating for carbon/carbon composites against ablation, Surf. Coat. Technol. 300 (2016) 1–9. https://doi.org/10.1016/j.surfcoat.2016.05.028.

[35] A. Kaiser, M. Lobert, R. Telle, Thermal stability of zircon (ZrSiO4), J. Eur. Ceram. Soc. 28 (2008) 2199–2211. https://doi.org/10.1016/j.jeurceramsoc.2007.12.040.

[36] W. Tan, M. Adducci, R. Trice, Evaluation of rare-earth modified ZrB2−SiC ablation resistance using an oxyacetylene torch, J. Am. Ceram. Soc. 97 (2014) 2639−2645. https://doi.org/10.1111/jace.12991.